Component analysis of 3D elastic 9C full waveform inversion: Ettlingen Line case study

T.M. Irnaka[1,4], *R. Brossier*[1], *L. Métivier*[2,1], *T. Bohlen*[3], *Y. Pan*[3]
[1] *Univ. Grenoble Alpes, ISTerre, F-38000 Grenoble, France*
[2] *Univ. Grenoble Alpes, CNRS, LJK, F-38000 Grenoble, France*
[3] *Geophysical Institute, Karlsruhe Institute of Technology, Germany*
[4] *Universitas Gadjah Mada, Yogyakarta, Indonesia*

SUMMARY

Full Waveform Inversion (FWI) is one of the most popular seismic imaging techniques. In the exploration scale, FWI has become one of the industrial standards and proven to be accurate. Following that trend, FWI in shallow seismic scale also starts to gain attraction in the past decade. Several publications have demonstrated and proposed workflow to tackle the challenges in shallow seismic scales, such as sparse and limited acquisition, weak signal to noise ratio, high complexity propagation due to the strong elastic effect, and strong attenuation. In this research, we focus on the analysis of the effect of multi-component data in shallow seismic scale towards 3D elastic FWI. The experiment's target is the Ettlingen Line (EL), a defensive trench-line which was built by the German Troop in 1707, located at Rheinstetten, Germany. We perform both synthetic (using cartesian direction's source) and field data (using Galperin source) in order to demonstrate the effect of multi-component data on FWI. Sixteen component combinations are analyzed for each case. By doing so, we find out that incorporating multi-component data generally has a positive impact on FWI in terms of model and data misfit, especially if the horizontal components are taken into account. The importance of each component can be used for future shallow seismic acquisition design for FWI with similar conditions.

INTRODUCTION

Full Waveform Inversion (FWI) is a high-resolution seismic imaging technique, based on an iterative data fitting procedure. It takes advantage of all recorded waveform in order to reconstruct the physical parameters of the subsurface. In the past decade, FWI starts to gain popularity in the shallow seismic community, despite being widely used in crustal-scale experiments (Virieux and Operto, 2009; Tromp, 2019). In general, FWI has becoming one of the standards of seismic imaging, even though there are still several challenges such as local minima, cycle skip, accurate physical modeling, and expensive computational cost. In shallow seismic scale, the challenges range from a typical single component dataset, sparse coverage or the targets due to the limited source and receiver, 2D rather than 3D acquisition, poor signal to noise ratio due to the weak seismic source, high complexity propagation due to the elastic effect, and strong attenuation. Several previous applications in shallow seismic data have been carried out to tackle those difficulties (Fathi et al., 2016; Nguyen and Tran, 2018; Smith et al., 2019; Wittkamp et al., 2018; Irnaka et al., 2019a).

Our experiment's target is the Ettlingen Line (EL), a defensive trench-line that was built by German troops during the War of the Spanish Succession in 1707 (Lang et al., 1907). This trench line is located in the city of Rheinstetten, southwest of Karlsruhe. It is close to the border between Germany and France. The trench is surrounded by the fluviatile sediment deposited from the Rhine River. The shape of the EL is an inverted triangle reinforced with the brushwoods and palisade woods. At the location of the experiment, the EL has been buried to the ground. Previously, several experiments have been performed on this site, such as GPR measurement and data analysis by (Wegscheider, 2017), 2D FWI using both Love and Rayleigh waves (Wittkamp et al., 2018), 3D MASW using the same dataset with this study (Pan et al., 2018), and 3D Elastic FWI (Irnaka et al., 2019a,b). GPR measurement reveals the inverted triangle shape of the target. In addition, previous MASW and 2D FWI experiments produce both the shape and the low-velocity anomaly of the target.

In this research, we focus on the analysis of multi-component data and its impact on 3D FWI. Previously, Smith et al. (2019) and Nuber et al. (2017) have shown that incorporating horizontal component is beneficial for the model reconstruction. In our field experiment, we use the Galperin source with the waves are excited along three orthogonal direction with an angle of 54.7° to the vertical axis (Häusler et al., 2018). Aside from performing the experiment on the field data, a synthetic study with a regular cartesian source direction is conducted to gain better understanding on the influence of the direction of the source. We analyze the result of the FWI, both qualitative and quantitatively, through the reconstructed model, model misfit, and data misfit.

FULL WAVEFORM INVERSION

The FWI is solved through a local minimization problem based on the least-squares misfit function ($\chi(m)$) which measure the discrepancy between the observed data (d_{obs}) and the synthetic data (d_{cal})

$$\chi(m) = \frac{1}{2} \left\| d_{cal}(m) - d_{obs} \right\|^2 . \quad (1)$$

We follow the l-BFGS technique, in order to update the physical parameter for each iteration (Byrd et al., 1995). The gradient is estimated using the adjoint-based formulation (Plessix, 2006). The elastic wave equation for the incident and the adjoint wavefield is solved using spectral element technique (Komatitsch et al., 2000; Trinh et al., 2019).

We use SEM46, a Fortran visco-elastic modeling and inversion tool based on spectral element method and SEISCOPE optimization toolbox (Métivier, 2014; Trinh et al., 2019). It offers automatic mesh building using a cartesian based mesh. SEM46 has two-levels parallelism using MPI, which are the parallelization over the source and the computational domain through domain decomposition.

In this application, we follow an FWI workflow for shallow seismic applications by Irnaka et al. (2019b). We consider multi-scale strategy FWI, starting from the lowest frequency band (3-15 Hz) to the higher frequency band (3-45 Hz) with the increment of 10 Hz at the high frequency for each scale. In order to be able to perform multi-parameter FWI, starting with a relatively simple model, and mitigating the strong elastic effect as the surface wave, we perform two consecutive FWI for each scale. The first FWI is a parameter binding FWI, where a hard-constraint is imposed on V_P with respect to V_S. During this process, the inversion is mainly driven by the update of V_S. It is due to the strong V_S sensitivity of the surface wave. The second FWI is a true multi-parameter FWI for V_P and V_S using non-linear parameter constraints. During this inversion, aside from having individual V_P and V_S boundary, we introduce another boundary constraint based on the Poisson's ratio.

APPLICATION

Data acquisition

The 3D dense seismic acquisitions have been performed within two weeks in April-May 2017. The experiment is led by Karlsruhe Institute of Technology, in collaboration with GFZ Potsdam, ETH Zurich, and Univ Grenoble Alpes. Figure 1a represents the acquisition design,

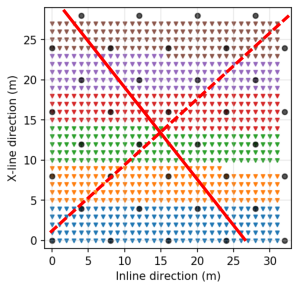

Figure 1: Layout of the acquisition grid. The total number of receiver is 888, the total number of source's location is 36. Solid and dashed red lines represent the parallel and perpendicular section on Figure 2, respectively.

10.1190/segam2020-3426088.1

with 36 source positions (black circles) and 888 receiver positions (inverted triangles). We use 3C geophones aligned with cartesian directions, and 3C source. The source is the Galperin Source (Häusler et al., 2018), a directional multi-component designed for the shallow seismic purposes. It is consists of 3C direction U,V,W where the setup and parameter can be seen on Irnaka et al. (2019a). It is aimed to have better ease of usage for shallow seismic field applications in terms of multi-component aspect, and consistent source-ground coupling (Fig. 1b). Different colors on the receiver's positions represent different days of acquisition. Before the application of FWI, a data correction based on the matching filter has been performed. This preprocessing step is essential in order to improve the consistency of the data (Irnaka et al., 2019a).

Experiment setup of multi-component analysis

3D Elastic FWI has produced a sufficiently good result for the EL using all 9C components up to 65 Hz (Irnaka et al., 2019a). During that application, we have not addressed the question regarding the impact of 9C FWI, and multi-component FWI in general, for FWI. In this research we analyze in detail multi-component FWI with various source and receiver component combination. We perform both field and synthetic aplication which have different source type. The aim of the synthetic test is not to mimic the field experiment, but to have a better physical understanding of the wavefield excited by point forces in the classical cartesian directions. The field data use the available source (Galperin) and receiver type. Whereas, the synthetic data has a cartesian direction source (Z, X, Y). The pseudo-observed data used in the synthetic test is calculated using 3D velocity model from the 9C FWI of the real field data up to 65 Hz. We believe this model is a good representation of the shallow seismic case.

We perform 16 different FWI with different component's combinations for both field data and synthetic case. Both experiments have homogeneous initial model. It consists of nine 1C FWI for each source and receiver component pair, three 3C FWI using multi-component receivers, three 3C FWI using multi-component sources, and one 9C FWI using all source and receiver components. The notation for 1C FWI is given as two letters; for example, UZ represents 1C FWI, using the U source component and vertical (Z) receiver component. The notation of 3C FWI is given as the component that is used during the FWI subscripted with the source or receiver side; for example, Z_{SRC} represents 3C FWI using only vertical (Z) source's component and all receiver's components.

The reconstructed V_S of the field data can be seen in Figure 2. For each subfigure, 16 different images are representing 16 different FWI. The rows represent the source's components, whereas the columns are the receiver's components. We display horizontal sections at 1.5 m deep, and two vertical slices which are perpendicular and parallel to the EL, respectively.

The result of both field and synthetic FWI experiments can be analyzed both qualitatively and quantitatively. Qualitative analysis is performed by evaluating the reconstructed model (Fig. 2). On the other hand, a quantitative analysis of each FWI result is done through model and data misfit.

Model misfit

We estimate the model misfit in order to compare the reconstructed model in this study quantitatively. The model misfit ($\mathscr{C}$) is calculated using weighted and normalized least-squares misfit

$$\mathscr{C} = \frac{1}{2}\left\| \frac{w(\overline{m_r} - m_t)}{\overline{m_r}} \right\|^2 \quad (2)$$

where $\overline{m_r}$ is the reference model, m_t is the target model calculated using each FWI, where w is the weight. The normalization is essential to estimate a relative misfit value for different parameter's range. The weight itself is determined using the uncertainty of the reference model (m_r).

There is not any exact true velocity model for the real field application. Therefore, the reference model is calculated by taking the mean of two previously reconstructed velocity models; which are obtained using FWI starting from two different initial models. One is started from the homogeneous model, the other is started from MASW model

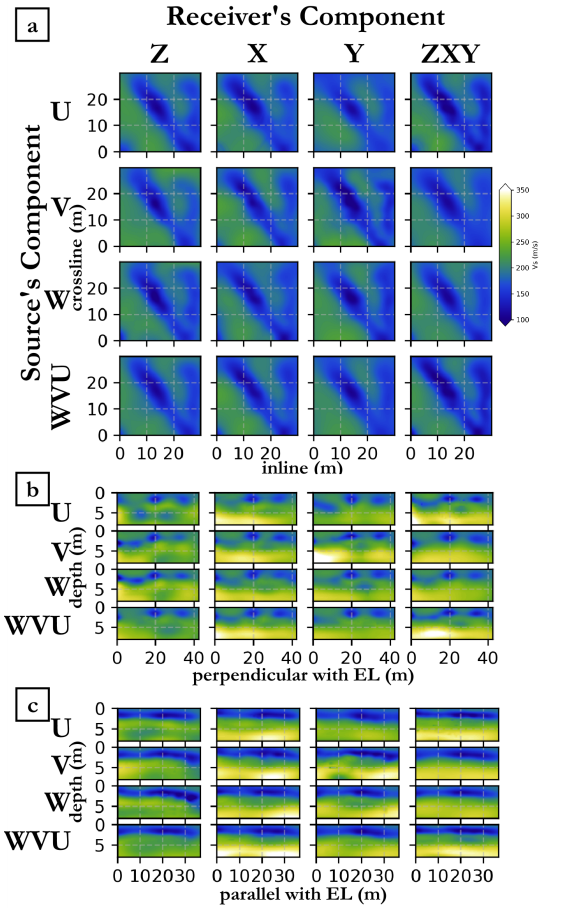

Figure 2: Reconstructed V_S from 16 FWI with various component combinations on field data application. The top figure (a) represents horizontal slice at 1.5 m, middle (b) and bottom right (c) figures represent the vertical slice perpendicular and parallel to the Ettlingen Line (EL), respectively. For each figure block, there are 16 different FWI, the rows represent the Galperin source's component, whereas the columns represent the receiver's component.

(Pan et al., 2018). The weight is then calculated as a function of depth ($w(z)$), inversely proportional to the standard deviation between the two models.

The reference model for the synthetic case is the reconstructed model from 9C FWI up to 65 Hz, which is initialized by the homogeneous model. Due to its nature, it has no uncertainty on the reference model leading to equal weight.

Data misfit

The data misfit is calculated using the least squares misfit by creating 9C synthetic seismic data based on each obtained model with the respective component combination. For better comparison, we used the same mesh design and time step for all models. For each case, we use the same source time function, retrieved using deconvolution formulation (Pratt, 1999) based on the velocity model on 9C FWI. In the end, for each FWI, we have nine disaggregated misfit values according to each component. Figure 4a and 7a shows the misfit matrix of all 16 FWI. Each separated block is a different FWI with different component's combination. The rows represent the source's components, whereas the columns represent the receiver's components. Each block contains a 3x3 color matrix, which corresponds to the source-receiver component's pair (the rows are source's component, whereas the columns are receiver's component).

Due to the content variability on each component, the absolute misfit value comparison between each component is not an excellent way to interpret. Therefore, we also provide the alternative view by comparing the data misfit of the same component on all 16 inversions and sort it

10.1190/segam2020-3426088.1

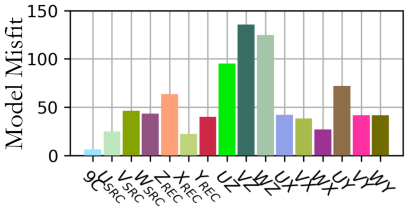

Figure 3: Weighted least-squares V_S model misfit for 9C and 3C FWI, and 1C FWI with respect to the reference model for the field data application. Model misfits which take into account horizontal component receiver give a significantly lower model misfit compared to the vertical one. FWI using 1C source and 3C receiver give relatively similar misfit, whereas FWI using 3C source and 1C receiver give lower misfit on the horizontal component receiver. The vertical only receiver (Z_{REC}) has higher misfit than the other 3C FWI but it has significantly lower misfit than 1C FWI using vertical component.

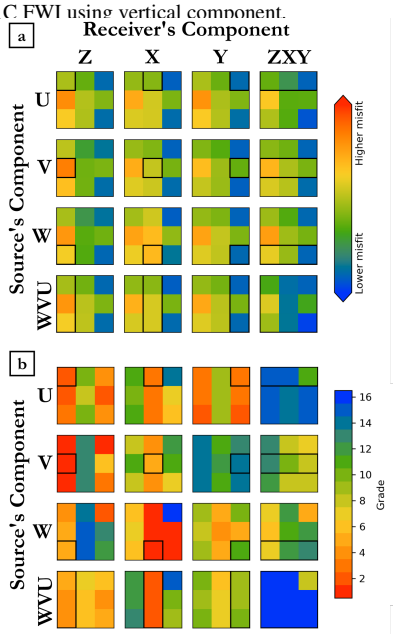

Figure 4: Color representation of the absolute misfit (a) and grade of component misfit (b) from all sources on the field data application. Each figure consists of 16 independent FWI with different component combination. For each FWI, we have a 3 by 3 matrix, the colors represent the misfit for each component (the rows are the sources' component, whereas the columns are the receivers' component.), the black rectangles represent the component combination which are used during the FWI. The absolute misfit matrix (a) represent the true calculated misfit value. Higher grade (b) means better data misfit compared to the same component on different FWI.

based on the misfit value (Fig. 4b and 7b). Higher grade means lower misfit value compared with the other component's combinations.

RESULT

Field experiment

The reconstructed V_S model obtained on the field data shows a consistent shape of the EL throughout 16 FWI. The EL can be seen as a low-velocity anomaly with northwest-southeast direction. Another trench line structure with north-south orientation is also reconstructed on all FWI. The lateral extension of both features can be clearly seen in the horizontal section of the image at a depth of 1.5 m (Fig. 2a). At this depth, the variability of the reconstructed models is relatively small. Visually, the FWI using 1C VY, 3C V, and 9C FWI provide better resolution, especially on the second trench-like structure, which is close to the edge of the model. The vertical section shows a consistent shape of the EL in all 16 FWI. It can be observed as the inverted triangle anomaly in Figure 2b. The depth of the target can be deducted from all FWI on the parallel section (Fig. 2b). The differences between reconstructed models are more observable at depth. Generally, the FWI, which takes into account the horizontal receiver's components (X and Y) can produce better model at depth compared to the FWI using only the vertical component. FWI using multi-component is also seen to have better model reconstruction close to the edge of the model, thanks to the potential increase of the data and illumination in that region.

The V_S model misfit on this field experiment shows the lowest value for 9C FWI with respect to the reference model (Fig. 3). Keeping in mind that one of the ingredients to build the reference model is the reconstructed model using 9C FWI at a higher frequency. The FWI application using 3C source and 3C receiver has a similar order of magnitude misfit function, even only using vertical components (Z_{REC}). Despite that, amongst the other 3C FWI, Z_{REC} has the highest model misfit value, which is corresponding to the lack of the ability to reconstruct the model at depth (see Fig. 2b and c). X_{REC} has the lowest 3C FWI model misfit, which also corresponds to the depth reconstruction in this experiment.

Model misfits on 1C FWI show significantly higher values for all vertical components (UZ, VZ, and WZ) compared to all horizontal receiver components. UY component has the highest model misfit amongst the horizontal receivers, potentially due to the off-plane propagation of the wave, hence reducing the sensitivity of the data. During this experiment, a multi-component approach might not improve the result dramatically if we take into account the horizontal component. Nonetheless, having data redundancy might lead to a more constrained inversion, especially in a more complex structure. The most significant improvement of model misfit occurs between 1C vertical receiver and 3C Z_{REC}, although we still miss the depth reconstruction of the image. Using this particular Galperin source and cartesian receiver, we show that the receiver's orientation selection plays an essential role in the FWI.

Figure 4a shows the absolute misfit on each component towards the respective FWI. Generally, all FWI produce similar patterns, emphasizing the relatively consistent convergence of the inversion. In this particular case, VZ components seem to have the highest misfit, and WY components have the lowest misfit on each FWI calculation.

The contribution of each component towards the FWI can be better examined in Figure 4b. This figure represents the grade of each component if it is compared with the same component on different FWI. For example, blue color (highest grade) means that using the specific component for FWI (indicated by a black rectangle) produces the lowest data misfit on a given component with color compared to the rest 16 FWI.

This component misfit's grade shows that taking into account a specific component does not mean that we have the best improvement on that particular component. These phenomena are observed on 1C FWI and 3C source FWI. One of the examples is the FWI using only VZ component (second row, first column). Even if we only use a single component during the FWI, the component X on the receiver can be moderately modeled compared to the other FWI. Unfortunately, the X component turns out to have a relatively less impact on the inversion. It can be seen from the model misfit value, where the VZ FWI has the highest misfit (Fig. 3). 3C receiver FWI shows a different trend where the component which is taken into account for the inversion, generally have better grade or improvement. Those two observations suggest the importance of the multi-component source and receiver. In this particular case, the multi-component receiver seems to have a more notable impact than the multi-component source.

Combining both multi-component sources and receivers has a significant impact on the FWI. In general, it yields the FWI with the best grade for almost all components, except UY. This result is possible because of the increase of illumination of the medium, as well as data redundancy. A significant improvement due to the data redundancy might as well observed on the 3C Z_{REC} FWI, where it has a much lower misfit despite using the vertical component receiver exclusively.

Synthetic experiment

The field experiment is limited to the available source and receiver component. With the synthetic experiment, we try to simulate the ex-

10.1190/segam2020-3426088.1

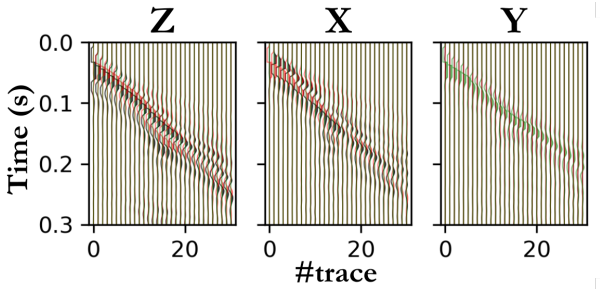

Figure 5: Synthetic data calculated using true velocity model on synthetic experiment. The source is located at position $x = 0$ m, and $y = 16$ m, and the receiver is located on inline direction at $y = 16$ m. Three subfigures represent different receiver's component, whereas the color on each figure represents source's component. Grey, red, and green seismograms are calculated using Z, X, and Y direction source, respectively.

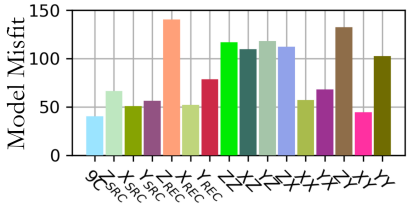

Figure 6: Weighted least-squares V_S model misfit for 9C and 3C FWI, and 1C FWI with respect to the reference model for the synthetic case. The behavior is similar compare to the field data, using horizontal component yield lower model misfit.

periment with a cartesian direction source and realistic model taken from the EL case. Figure 5 shows an example of the synthetic seismogram for this synthetic experiment showing a strong surface wave footprint. With this particular setup, model misfits on 3C FWI have similar value and even close to 9C FWI, except for 3C Z_{REC} FWI. The FWI using only vertical receiver's component are shown to produce the highest model misfit, aligned with the result on the field data (Fig. 6). This observation is likely due to the strong presence of the horizontal component towards the Love wave and the radial component of the Rayleigh wave. The model misfits on the 1C FWI show an interesting result. The model misfit exhibits a relatively higher misfit when we take into account the Z component, both on source or receiver. These observations render only three ideal component combinations for 1C FWI (XX, YX, XY). YY has relatively high model misfit due to the lack of illumination, at some part of the model close to the edge. It can be seen by a good match in terms of data fit but relatively high model misfit. This phenomenon can be avoided when we take into account multi-component data. On the field experiment, there is no pure vertical source, in which the similar behavior might occur as well. Observing the model misfit on the synthetic model gives us the emphasis on the importance of the horizontal component source and receiver, as well as the benefit of having an oriented source (such as Galperin source).

The absolute data misfit on this the synthetic case shows that the total misfits are dominated by three main components (ZZ, XX, and YY). Those three components have up to 10 times higher absolute misfit value compared to the other components. Figure 7c shows how some components are dominant and might be more influential to the model reconstruction. The absolute data misfit plot (Fig. 7a) has already given a clear picture that the FWI with the horizontal component yield better data misfit. The grade of component misfit shows that the multi-component FWI, especially 9C and multi-component receiver, provides a natural balance between the data fit of the different components (Fig. 6).

CONCLUSION

FWI has been shown to provide a high-resolution subsurface model. The workflow that we follow is proven to be stable for this particular case. It is shown by the relatively consistent result throughout the

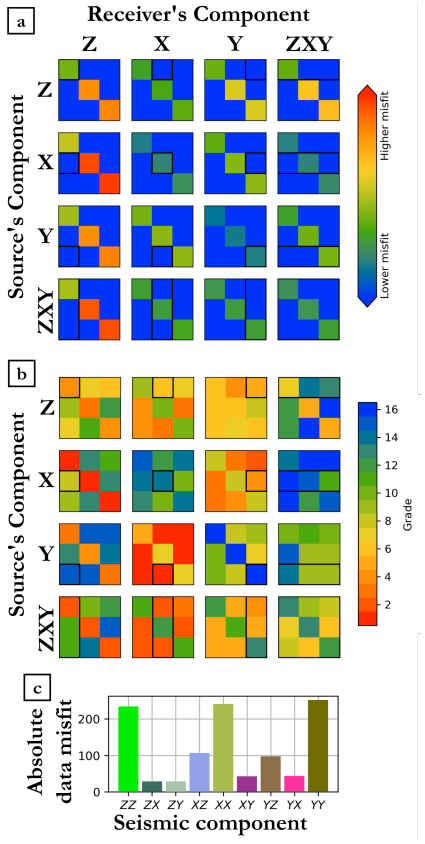

Figure 7: Color representation of the absolute misfit (a) and grade of component misfit (b) from all sources on the field data application. The layout is similar compared to Figure 4. Bar plot of the absolute data misfit on 9C FWI (c).

test using the different component combinations. Several minor details on the reconstructed model can be associated with the impact of the component used during the FWI. We show, through model and data misfit, the contribution of each component combination towards FWI. The horizontal components provide a crucial contribution to shallow seismic imaging at depth. It is related to the more substantial presence of the Love wave and the radial component of the Rayleigh wave. We also show that a multi-component receiver has a more significant impact than multi-component source, which can be considered for future seismic acquisition design. This study also puts an emphasis that having multi-component data (either source or receiver) almost always give us better model reconstruction, especially if any horizontal component can be taken into account. Multi-component oriented sources (e.g., Galperin source, Prismatic source) also play an essential role in distributing the energy of the source to the multi-component receiver. Despite that, even with the limited equipment, 1C source and receiver can still potentially produce a good result (mainly on XX, XY, and YX), as shown in the synthetic case. This information can also be useful for future shallow seismic acquisition design.

In the following research, we would like to investigate the effect of the source's and receiver's sparsity and analyze the benefit of multi-component data in such a scenario.

ACKNOWLEDGEMENTS

This study was partially funded by the SEISCOPE consortium (`https://seiscope2.osug.fr`), sponsored by AKERBP, CGG, CHEVRON, EQUINOR, EXXON-MOBIL, JGI, PETROBRAS, SCHLUMBERGER, SHELL, SINOPEC, SISPROBE and TOTAL; also partial financial support by the Deutsche Forschungsgemeinschaft (DFG) with project-ID 258734477-SFB 1173. This study was granted access to the HPC resources of CIMENT infrastructure (`https://ciment.ujf-grenoble.fr`) and CINES/IDRIS/TGCC under the allocation 046091 made by GENCI.

10.1190/segam2020-3426088.1

REFERENCES

Byrd, R. H., P. Lu, and J. Nocedal, 1995, A limited memory algorithm for bound constrained optimization: SIAM Journal on Scientific and Statistical Computing, **16**, 1190–1208, doi: https://doi.org/10.1137/0916069.

Fathi, A., B. Poursartip, K. H. Stokoe II, and L. F. Kallivokas, 2016, Three-dimensional P-and S-wave velocity profiling of geotechnical sites using full-waveform inversion driven by field data: Soil Dynamics and Earthquake Engineering, **87**, 63–81, doi: https://doi.org/10.1016/j.soildyn.2016.04.010.

Hausler, M., C. Schmelzbach, and D. Sollberger, 2018, The Galperin source: A novel efficient multicomponent seismic source: Geophysics, **83**, P19–P27, doi: https://doi.org/10.1190/geo2018-0020.1.

Irnaka, T., R. Brossier, L. Métivier, T. Bohlen, and Y. Pan, 2019a, Towards 3D 9C elastic full waveform inversion of shallow seismic wavefields - case study Ettlingen Line: 81th Annual International Conference and Exhibition, EAGE, Expanded Abstracts, EAGE, We P01 04, doi: https://doi.org/10.3997/2214-4609.201900994.

Irnaka, T. M., R. Brossier, L. Métivier, T. Bohlen, and Y. Pan, 2019b, Uncovering the effect of multi-component data on 9C 3D elastic FWI: Ettlingen Line case study: AGUFM, S31D–0565.

Komatitsch, D., C. Barnes, and J. Tromp, 2000, Simulation of anisotropic wave propagation based upon a spectral element method: Geophysics, **65**, 1251–1260, doi: https://doi.org/10.1190/1.1444816.

Lang, K., et al., 1907, Die ettlinger linien und ihre geschichte: Selbstverlag der Stadt Ettlingen.

Métivier, L., 2014, SEISCOPE optimization toolbox manual: Technical Report code version 1.0, SEISCOPE project.

Nguyen, T. D., and K. T. Tran, 2018, Site characterization with 3D elastic full-waveform tomography: Geophysics, **83**, R389–R400, doi: https://doi.org/10.1190/geo2017-0571.1.

Nuber, A., E. Manukyan, and H. Maurer, 2017, Optimizing measurement geometry for seismic near-surface full waveform inversion: Geophysical Journal International, **210**, 1909–1921, doi: https://doi.org/10.1093/gji/ggx267.

Pan, Y., S. Schaneng, T. Steinweg, and T. Bohlen, 2018, Estimating s-wave velocities from 3D 9-component shallow seismic data using local Rayleigh-wave dispersion curves – a field study: Journal of Applied Geophysics, **159**, 532–539, doi: https://doi.org/10.1016/j.jappgeo.2018.09.037.

Plessix, R. E., 2006, A review of the adjoint-state method for computing the gradient of a functional with geophysical applications: Geophysical Journal International, **167**, 495–503, doi: https://doi.org/10.1111/j.1365-246X.2006.02978.x.

Pratt, R. G., 1999, Seismic waveform inversion in the frequency domain, Part I: theory and verification in a physical scale model: Geophysics, **64**, 888–901, doi: https://doi.org/10.1190/1.1444597.

Smith, J. A., D. Borisov, H. Cudney, R. D. Miller, R. Modrak, M. Moran, S. L. Peterie, S. D. Sloan, J. Tromp, and Y. Wang, 2019, Tunnel detection at Yuma proving ground, Arizona, USA—Part 2: 3D full-waveform inversion experiments tunnel detection at YPG—part 2: 3D FWI: Geophysics, **84**, B95–B108, doi: https://doi.org/10.1190/geo2018-0598.1.

Trinh, P. T., R. Brossier, L. Métivier, L. Tavard, and J. Virieux, 2019, Efficient 3D time-domain elastic and viscoelastic Full Waveform Inversion using a spectral-element method on flexible Cartesian-based mesh: Geophysics, **84**, R75–R97, doi: https://doi.org/10.1190/geo2018-0059.1.

Tromp, J., 2019, Seismic wavefield imaging of earth's interior across scales: Nature Reviews Earth and Environment, 1–14.

Virieux, J., and S. Operto, 2009, An overview of full waveform inversion in exploration geophysics: Geophysics, **74**, WCC1–WCC26, doi: https://doi.org/10.1190/1.3238367.

Wegscheider, S., 2017, Abbildung der ettlinger linie auf dem segelflugplatz rheinstetten mittels georadar: Master's thesis: Karlsruhe Institute of Technology.

Wittkamp, F., N. Athanasopoulos, and T. Bohlen, 2018, Individual and joint 2-D elastic full-waveform inversion of Rayleigh and Love waves: Geophysical Journal International, **216**, 350–364, doi: https://doi.org/10.1093/gji/ggy432.